Supramolecular association of (1,4-phenylenedimethanaminium) bis(perchlorate) monohydrate: A Combined Experimental and Theoretical Study

Ikram Jomaa, Chaima Daghar, Noureddine Issaoui, Thierry Roisnel, Houda Marouani

Supramolecular association of (1,4-phenylenedimethanaminium) bis(perchlorate) monohydrate: A Combined Experimental and Theoretical Study

Ikram Jomaa[a], Chaima Daghar[a], Noureddine Issaoui[b], Thierry Roisnel[c], Houda Marouani[a,*]

(a) Université de Carthage, Faculté des Sciences de Bizerte, LR13ES08 Laboratoire de Chimie des Matériaux, 7021, Zarzouna, Bizerte, Tunisie

(b) University of Monastir, Laboratory of Quantum and Statistical Physics LR18ES18, Faculty of Sciences Manastir, 5079, Tunisia

(c) Univ Rennes, CNRS, ISCR (Institut des Sciences de Rennes) – UMR 6226, F 35000 Rennes, France

* Correspondence e-mail : houdamarouani2015@gmail.com

Highlights

- Structure elucidation of a novel perchlorate compound.
- The atomic arrangement shows a three-dimensional network.
- Active sites were explained using MEP, Hirshfeld, and HOMO-LUMO studies.
- Good agreement was found between DFT findings and experimental data.

Graphical abstract

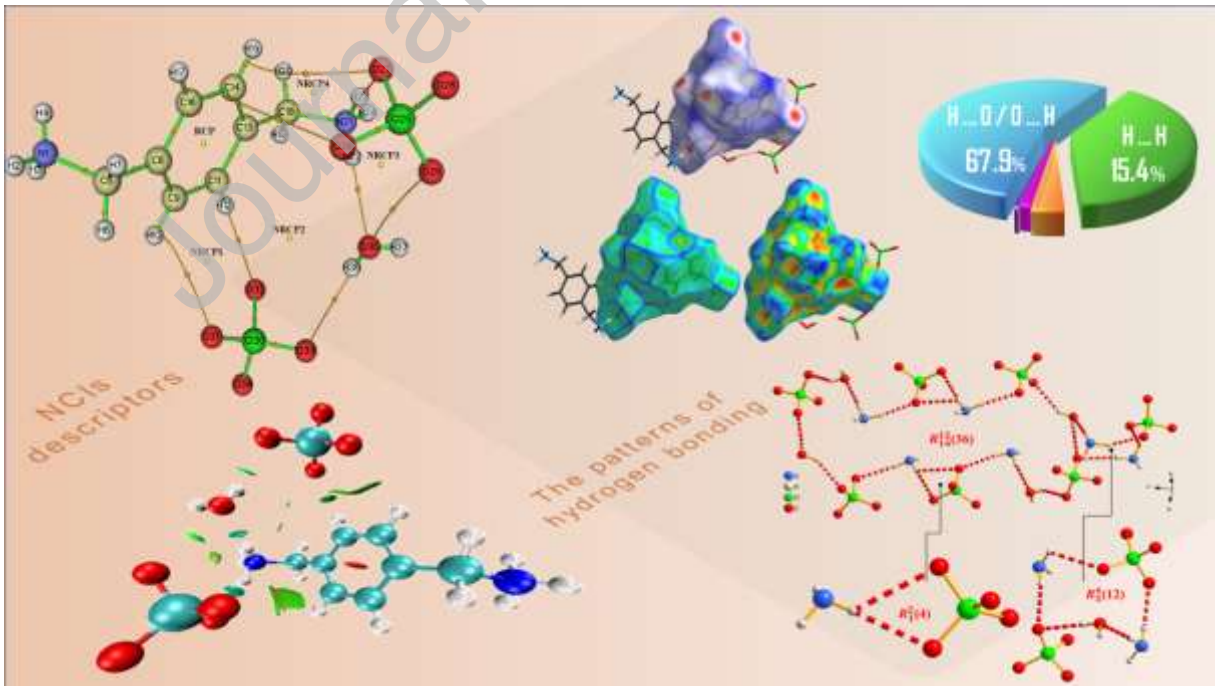

Abstract

This paper deals with the crystal structure of the new material (1,4-phenylenedimethanaminium) bis(perchlorate) monohydrate, $(C_8H_{14}N_2)(ClO_4)_2 \cdot H_2O$ that was prepared in crystalline form by solvent evaporation method at room temperature. Single crystal X-ray diffraction analysis shows that this compound crystallizes in the monoclinic system, with the space group $P2_1/c$. The title structure benefits from extensive intermolecular interactions such as C-H… π interactions and hydrogen bonds which are the major forces to make it more stable in the solid-state.

The interactions in the solid-state have been also studied using Hirshfeld surface analyses (d_{norm}, curvedness, and shape index), as well as its 2D fingerprint plots. To reinforce experimental results, DFT calculations have been performed via the B3LYP/LanL2DZ method. HOMO-LUMO energies and the chemical quantum descriptors were taken into account. AIM and RDG analysis has been explored to reveal the steadiness of the molecule. Molecular electrostatic potential inspection has also been submitted in the study.

Keywords: Crystal structure, DFT calculations, Hirshfeld surface, Vibrational study, AIM.

1. Introduction

A long-standing interest was devoted to the structural chemistry of diammonium cations type and to their hydrogen bonding schemes **[1-4].** Here one of the Xylylenediamine derivatives which are well-known diamines that incorporates everalalluring biological and notably anti-microbial properties, will be the candidate for the organic counterpart. In fact, the inhibition activity against a panel of microbes such as: *Escherichia coli, Enterococcusfaecalis, Pseudomonas aeruginosa, Pseudomonas exotoxin, Klebsiellapneumoniae, Staphylococcus epidermidis, Bacillus subtilis*,..etc was deliberated in two separate papers through an in vitro study **[5]** and in an in silico investigation **[6]**. Furthermore, there are already some Xylylenediamine derivatives with simple counter anions that have been reported in the literature namely: p-xylylenediaminium bis(nitrate) **[7]** (m-Phenylenedimethylene)diammonium dichloride **[8]** m-xylylenediaminium bis(perchlorate) monohydrate **[9]**.

Other than that, perchlorate salts have been extensively reviewed since 1997 when they were first identified in a water source **[10]** and in other supplies: drinking water **[11]**, food, milk **[12]**, soil, corns **[13,14]**,…etc. Perchlorates (ClO_4^-) are high-performance materials

due to their interesting physicochemical properties and their high solubility and poor adsorption **[15]**.

Non metal cation perchlorate salts can be considered hybrids compounds of type I in which the inorganic moiety is metals deficient. From a structural point of view, perchlorate-organic assembly enables a great variety of structural archetypes to be constructed in the form of clusters or infinite chains **[16]** with the water molecules in hydrated compounds. For all these reasons, it seemed interesting to study this family of non-metal perchlorate hybrids.

The present contribution is intended to report the crystal structure in detail of the new hybrid compound p-xylylenediaminium bis(perchlorate) monohydrate, the Hirshfeld surface analysis along with fingerprints plots calculations and the associated enrichment ratio. Other computational analyses will be as well presented including the molecular electrostatic potential (MEP), frontier orbitals (HOMO-LUMO), topological properties approach (AIM and RDG).

2. Experimental section

2.1. Chemical preparation

All reagents: The cadmate chloride monohydrate (purity 98%), perchloric acid $HClO_4$ (purity 96%), and 1,4-Phenylenedimethanamine (purity 96%), were used as received from Sigma-Aldrich, without further purification. The title compound was obtained by mixing at ambient conditions:

A solution of 1,4-Phenylenedimethanamine (2mmol, 0.2 g) dissolved in 10 mL of deionized water, and $CdCl_2.H_2O$ (1 mmol, 0.1 g) mixed in dilute perchloric acid (2mmol, 0.2 g) that was carefully added under continuous stirring. One week later well-defined single crystals suitable for single crystal X-ray structure analysis were formed.

Elemental analysis, calc. (found): C, 27.04% (27,70); H, 4.50% (5,31); N, 7.88% (7,81).

2.2. X-ray data collection and physical measurements

A single crystal of $(C_8H_{14}N_2)(ClO_4)_2{\cdot}H_2O$ with good quality and suitable size was selected in order to perform its structural analysis. Data were collected on a D8 VENTURE Bruker AXS diffractometer at 150 K using a Multi layer monochromator and MoKα radiation (λ= 0.71073 Å). Absorption corrections were performed using the multi-scan technique and the SADABS program **[17]**. The total number of measured reflections was 8363 of which 3265, were

independent and 2788 with the intensity $I > 2\ \sigma(I)$. The structure was solved with SHELXT **[18]**, which displayed the position of all non-hydrogen atoms and then refined with full-matrix least-square method founded on F^2 (SHELXL) **[19]** incorporated in the WINGX program **[20].** A final refinement on F^2 converged at $R(F^2) = 0.035$ and $wR(F^2) = 0.128$. Crystal data and experimental parameters used for the intensity data collection are summarized in **Table 1**. Structure graphics are drawn with DIAMOND program **[21].** The Fourier Transform Infrared (FTIR) spectrum was registered with a Perkin-Elmer FT-IR 1000 spectrometer equipped with a diamond micro-ATR access, the scanning range was 4000–400 cm^{-1}.

2.3. Computational details

Initially, the crystallographic information file (CIF) of $(C_8H_{14}N_2)(ClO_4)_2{\cdot}H_2O$ compound was used as an input file, the molecular geometry optimization has been performed with the Gaussian 09 software package **[22]** and the Gauss-View molecular visualization program **[23]**. All the theoretical calculations have been performed via the hybrid B3LYP functional combined with the Lee-Yang-Parr correlation functional levels **[24,25]** and the LANL2DZ basis set. 3D Hirshfeld surfaces and 2D fingerprint were generated and based as well on the CIF format using Crystal Explorer software, version 3.1 **[26].**

The topological properties at the BCPs were determined with the Multiwfn program **[27]**, and the reduced density gradient analysis was made by the Multiwfn and the VMD programs **[28]**. The optimized molecular structure is used to perform HOMO-LUMO distributions and MEP analysis as well as Electron localization function and Local orbital locator inspection.

3. Results and discussion

3.1. Structure description and molecular modeling

As shown in (**Fig. 1a**), the asymmetric unit of $(C_8H_{14}N_2)(ClO_4)_2{\cdot}H_2O$ is formed by one dication doubly protonated at the N1 and N10 nitrogen atoms, two perchlorate anions, and one water molecule. The optimized geometric model of the structure is shown in **Fig. 1b.** The packing of $(C_8H_{14}N_2)(ClO_4)_2{\cdot}H_2O$, in the bc plane (**Fig. 2a**), shows that the compound is built up by a succession of cationic and anionic entities which alternate along the c-axis. In the partial view of the crystal structure **(Fig. 2b)** the anions and the bridging water molecules interact through hydrogen bonds to produce a corrugated chain. Perchlorate groups, $Cl1O_4$, are discrete and $Cl2O_4$ ones form with water molecules $C_2^2(6)$ corrugated channels extending

along the b-axis at z=¼ and z= ¾. Bond lengths and bond angles of the perchlorate anions and the 1,4-phenylenedimethanaminium cation are in the range of expectations compared to the literature **[30-34]** and to the calculated values using the B3LYP/LanL2DZ method (**Table 2**). The Cl–O bond lengths range from 1.419 (3) to 1.441 (2)Å, while the O–Cl–O angles range from 106.96 (16)° to 111.57 (19)°. The distortion indices of the different angles and bonds in the perchlorate tetrahedra based on the Baur method are [DI(Cl1O)= 0.0040, DI(OCl1O)= 0.0102 and DI(OO)= 0.0063 for $Cl1O_4$ and [DI(Cl2O)= 0.0043, DI(OCl2O)= 0.0058 and DI(OO)= 0.0033 for $Cl2O_4$. A sturdy distortion is noticed in O-Cl1-O angles if compared to the Cl-O, O-O distances and O-Cl2-O angles. It is clear from these values that the ClO_4 tetrahedron exists as a regular arrangement of oxygen atoms and that the chlorine atoms are displaced from the tetrahedral center of gravity [δCl1= 0.020; δCl2= 0.015]. For the 1,4-phenylenedimethanaminium cation there are already some salt structures listed in the Cambridge Structural Database with simple counter anions like: chloride **[32]** and Bromide **[33].** The aromatics C–C distances in the 1,4-phenylenedimethanaminium cations range from 1.383 (4) to 1.392 (4) Å, the aliphatic C–C distances range from 1.499 (4) Å to 1.508(2) Å and the N–C bonds are between 1.487 (4) and 1.491 (4) Å. Assessment of C-C-C and N-C-C angles shows significant alikeness with the compounds quoted above. The 1,4-phenylenedimethanaminium cations and perchlorates can form hydrogen-bonded and cross-linked networks. Thus, both ammonium groups in 1,4-phenylenedimethanaminium cation adopt a trans conformation, that was already observed in other compounds assembled with the identical organic cation **[7,34]**. The title structure shows the proficiency of semi-flexible organic cations to boost the formation of an ordered crystalline material by its conformational adjustments to style a maximum of hydrogen bonds. In **Fig. 3a**, where the packing of the studied compound was projected on the c-axis, the interlayer spaces of the organic groups that are in zig-zag distribution are filled with intercalated inorganic layers. The junction of both layers is governed, by three types of H-bonds, therefore forming the three-dimensional infinite network. The ammonium group N1 forms normal, bi and trifurcated N-H…O hydrogen bonds with only perchlorate anion of donor-acceptor distances varying between 2.856 (4) and 3.133 (4)Å. Whereas, the ammonium group N10 forms non-bifurcated N-H…O (OW) hydrogen bonds with water molecules and perchlorate anions. The C-H…O and OW-H…O hydrogen bonds along with the quoted above generate three different ring types (**Fig. 3b**) $R_{14}^{12}(36)$, $R_5^4(12)$ and $R_1^2(4)$. Organic cations are also close enough to enable two types of C–H…π interactions to occur with a distance of 3.812 Å and 3.849 Å that connect in a chain along a-axis (**Fig. 3c**).

3.2. Hirshfeld surface survey

Currently, Hirshfeld surface (HS) analysis **[35-38]** represents an enormous interest in the field of crystallography, as a complementary methodology for the examination of intermolecular interactions.

Hirshfeld surface investigation is a systematic computational approach that provides a virtual image where the different calculated types of interactions are clearly identified by the shapes, outlines, colors and color intensities, which are related to the relative strength of the interactions and to the short or long contacts. **Fig.4a** is a graph of the d_{norm} map that illustrates the relative positions of neighboring atoms belonging to molecules that interact with each other. The red spots highlight the interatomic contacts including the N—H···O, C—H…O and O—H…O hydrogen bonds. Curvedness and Shape-index plots of the Hirshfeld surface are both tools to visualize the C–H…π stacking by the presence of adjacent red and blue triangles in the shape-index graph and large flat regions delimited by a blue outline around the aromatic nuclei on the Curvedness graph. **Fig.4b** and **c** clearly suggest that C–H…π interactions are present in the title compound.

The 2D fingerprint plots of the intermolecular contacts of the title compound are shown in **Fig.S1**, the examination of the decomposed intermolecular interactions allows the quantification of individual contributions and display pairs of atoms in close contact. Further, the enrichment ratio was calculated to emphasize the contacts statistically favored in the crystal packing. The calculated values of the enrichment ratios in the title compound are given in **Table S1**. In fact, As expected, the enormous contribution (67.9%) comes from H…O/O…H intercontacts with a maximum sum of $d_e + d_i$ ~2.04 Å less than the sum of the VdW radii of the oxygen atom and the hydrogen atom (1.52 + 1.09 = 2.61 Å) thereby they are considered as close contact. The value (ER_{HO} = 1.53) greater than unity, of H…O /O…H contacts, reveals the tendency to assemble N—H···O, C—H…O and O—H…O hydrogen bonds. This finding was demonstrated by a structural X-ray analysis. H…H contacts comprise 15.4% of the entire HS and correspond to ($d_e + d_i$ ~2.43 Å), a value greater than the sum of the VdW radii of the atoms of hydrogen (H: 1.09 Å). This reveals the absence of close H…H contacts. The contacts H…C/C…H are privileged in a sample of aromatic molecules with (ER_{CH} = 1.62; this significant value (> 0.8) marks the presence of C–H… π interactions **[39].** H…C/C…H contacts show on its 2D graph the presence of symmetric pair of wings around a sum ($d_e + d_i$~ 2.91 Å) value greater than the sum of the VdW radii of hydrogen and carbon

atoms (2.79 Å) which exclude these contacts from being close. The O …O contacts are also visible on the HS (7%) and enriched with an enrichment ratio ER_{OO} = 0.41.

3.3. Vibrational FT-IR spectrophotometry and assignments

The vibrational properties of $(C_8H_{14}N_2)(ClO_4)_2{\cdot}H_2O$ hybrid material were discussed based on a vibrational study employing experimental infrared spectroscopy. The experimental IR spectrum measured between 4000 and 400 cm^{-1} is shown in **Fig. 5**. A preliminary assignment of the observed bands may be proposed, based essentially on comparison with previous works reported on perchlorate compounds **[9,40-43].** The N–H asymmetric and symmetric stretching vibration of the disubstituted aromatic ring is located in the high-frequency region between 3554-3501 cm^{-1}. The band observed at 1605 cm^{-1} is assigned to the asymmetric stretching mode of NH_3^+ and the symmetric mode is assigned to the band at 1491 cm^{-1}. The asymmetric and symmetric stretching vibrations of CH_2 are observed at 3065 and 2959 cm^{-1} respectively. The C=C stretching vibration appears at 1385 cm^{-1}. The strain band located at 839 cm^{-1} corresponds to the C-H out-of-plane bending vibration and shows the existence of a –1,4-disubstitution in $(C_8H_{14}N_2)(ClO_4)_2{\cdot}H_2O$ compound, C-N stretching vibration and asymmetric and symmetric C-C stretching modes are observed nearly in the same spectral domain.

Concerning the inorganic entity, the intense peak observed at 1074 cm^{-1} is assigned to the asymmetric stretching modes $\nu_{as}(ClO_4^-)$. Whereas, the band appearing near 839 cm^{-1} corresponds to the symmetric stretching mode $\nu_s(ClO_4^-)$. The bands appearing at 553 and 622 cm^{-1} correspond to the symmetric and asymmetric bending mode of ClO_4^-.

3.4. Quantum theory of AIMs analysis

The Quantum theory of atoms in molecules (QTAIM) was introduced by Bader **[44]**. It has been applied to analyze the nature of interactions between two compounds mainly hydrogen bonds. According to Bader each chemical bond has a critical point, denoted "BCP" and at this point, several topological parameters can be calculated, such as the electron density ρ(r), the Laplacian values $\nabla^2\rho(r)$, the ellipticity (ε), kinetic energy density (G), potential energy density V(r), Kinetic energy of Hamiltonian H(r) = G(r) + V(r) and the binding energy E_{int} = V(r)/2. All these parameters are listed and calculated in **Table 4** using the Multiwfn software **[45]** while the graphical representation of atom in molecule analysis of the compound is mapped in **Fig. 6**.

The calculated results indicate that the $\nabla^2\rho$ values are all positive and range from 0.0009 to 0.0226 a.u. indicate a depletion of electron density along with the bond path, which is

characteristic of closed-shell interactions like hydrogen bonding and particularly according to Rozas et al. **[46]** the Laplacian and the energy density values are positive therefore the six hydrogen bonds observed are considered weak.

In addition, the presence of a critical point in the RCP, NRCP1, NRCP2, NRCP3 and NRCP4 cycles confirms the cyclic nature of $(C_8H_{14}N_2)(ClO_4)_2 \cdot H_2O$ while RCP corresponds to the phenyl ring and NRCP are formed by the interactions between the organic group and the perchlorate group via hydrogen bonds. The low value of ellipticity (-1.2075) at the RCP point confirms that there is delocalization of the electron in the aromatic nucleus.

3.5. Reduced density gradient (RDG) analysis

The non-covalent interactions computational tool (RDG) is used to identify and understand the weak interactions between the different entities and it is based upon the reduced density gradient (RDG). In addition, the (RDG) **[47-48]** can be expressed as:

$$RDG(r) = \frac{1}{2(3\pi^2)^{1/3}} \frac{|\sigma\rho(r)|}{\rho(r)^{4/3}}$$

The illustration of various interactions types in $(C_8H_{14}N_2)(ClO_4)_2 \cdot H_2O$ is shown in **Fig. 7a.b.** The scatter plot of reduced-density gradient (RDG) and the sign $(\lambda_2)\rho(r)$ permit the assessment of the nature of interactions, the blue colors indicate the hydrogen-bonding interaction where the sign $(\lambda 2)\rho$ is negative, green colors correspond to the van der Waals interaction where the sign $(\lambda 2)\rho$ is close to zero, and the red color is defined as strong repulsion (steric effect) where the sign $(\lambda 2)\rho$ is positive. Regarding the isosurface color scheme in **Fig. 7.a**, an elliptical red plate is seen in the center of the aromatic nucleus related to a strong repulsion. Van der Waals interactions were seen between water, perchlorate and p-xylylenediaminium.

3.6. Molecular electrostatic potential surface

The molecular electrostatic potential (MEP) is a very useful descriptor for examining the intermolecular hydrogen bonding present in the compound. The MEP surface displays a color scheme where red is assigned to the negative charge (electron-rich), blue is assigned to the positive charge (electron-deficient), slightly blue where the region is slightly electron-deficient and yellow where the region is slightly electron-rich. As can be seen from **Fig. 8**, the region with negative potential is located in the perchlorate group and oxygen and is reflected as a yellow color. Also, the regions having the positive potential are over the hydrogen atoms of the ammonium group and are reflected as a blue color. Positive and negative potentials

sites provide information about the formation of intermolecular hydrogen bonding interactions **[49]**.

3.7. Frontier Molecular Orbital Energies

Molecular orbitals energies studies provide useful information on the electronic structure and chemical stability. The HOMO-LUMO and HOMO-1-LUMO+1 frontier orbital energies calculated with the DFT/6-311G orbital energy level are shown in **Fig. 9.** This figure shows that HOMO components are mainly localized on nitrogen, oxygen and benzene ring. LUMO components are mainly localized on ClO_4 group. The positive and the negative regions are represented by the red and the green colors. The energy gap between HOMO and LUMO orbitals is equal to 3.05 eV and the energy gap between HOMO-1 and LUMO+1 is equal to 3.76 eV which represents the electrical conductivity of $(C_8H_{14}N_2)(ClO_4)_2{\cdot}H_2O$. It is well known that a large gap indicates high stability and low chemical reactivity.

Parameters related to HOMO and LUMO such as the chemical hardness ($\eta = (I - A)/2$), the global softness ($S = 1/2\eta$), the electron affinity ($I = -E_{HOMO}$**),** the ionization potential ($A = -E_{LUMO}$), the global chemical potential ($\mu = -(I + A)/2$), the global electrophilicity ($\omega = \mu^2/\eta$) **[50]** and the electronegativity ($\chi = (I + A)$ **[51]** and the calculated results are listed in **Table S2**. The electronegativity χ = 6.1 eV and the global hardness η = 1.53 eV indicate the molecular capability of accepting electrons. Besides the negative value of chemical potential (μ= - 6.1 eV) reveals that the structure is stable. Moreover, the high ionization potential (I = 7.62 eV) indicates low reactivity in the system.

4. Conclusion

The present contribution is intended to shed light on the non-covalent weak interactions of the novel perchlorate compound, $(C_8H_{14}N_2)(ClO_4)_2{\cdot}H_2O$. A structural description has shown that the atomic arrangement forms a three-dimensional infinite network where organic cations, perchlorate anions, and water molecules are linked together via N-H…O, C-H…O, and OW-H…O H bonds. The entire supramolecular self-assembly of weak noncovalent interactions has been analyzed in detail (AIM, RDG, and MEP analysis) and further quantified by theoretical Hirshfeld surface analysis. Density functional theory (DFT) at the B3LYP/LanL2DZ level of theory was used to determine the ground-state optimized geometry, the calculated geometric parameters are in good line with the experimental data, and thus the entire theoretical investigations support the experimental findings. The HOMO and LUMO energies and other calculated quantum parameters reveal the hardness and the

great stability of the material. The vibrational wavenumbers of the fundamental modes have been precisely analyzed, and assigned by comparison with the vibration modes frequencies of homologous compounds.

Acknowledgements

We are grateful to the Tunisian Ministry of Higher Education Scientific Research for the provided support.

AUTHOR CONTRIBUTION STATEMENTS

Ikram Jomaa: Formal analysis and Writing
Chaima Daghar: Formal analysis and Writing
Noureddine Issaoui: Software
Thierry Roisnel: Software
Houda Marouani: Supervision and Validation

Declaration of interests

The authors declare that they have no known competing financial interests or personal relationships that could have appeared to influence the work reported in this paper.

References

[1] G.J. Reiss, Crystal structure of bis(1,3-phenylenedimethanaminium) bis(triiodide) tetraiodide–water (1/2) , $C_8H_{16}I_5N_2O$, Z. Kristallogr. New Cryst. Struct. 235 (2020)1047-1050.

[2] N. Brandt, G.J. Reiss, The twinned crystal structure of 1,3-phenylenedimethanaminiumdibromide, $C_8H_{14}Br_2N_2$, Z. Kristallogr. New Cryst. Struct. 236(2021) 519–521.

[3] C. Ben Mleh, T. Roisnel, H. Marouani, Synthesis and crystal structure of a new2,6-dimethyl piperazine-1,4-diium perchlorate monohydrate:$(C_6H_{16}N_2)(ClO_4)_2.H_2O$, Crystallogr. Rep. 62 (2017) 246-248.

[4] M. Tahenti, S. Gatfaoui, N. Issaoui, T. Roisnel, H. Marouani, A tetrachlorocobaltate(II) salt with 2-amino-5-picolinium: synthesis, theoretical and experimental characterization, J. Mol. Struct. 1207 (2020) 127781.

[5] V. Murugesan, M. Saravanabhavan, M. Sekar, Synthesis, spectral, structural characterization and biological investigation of m-Xylylenediaminium bis(ptoluenesulfonate) monohydrate, J. Photochem. Photobiol., B 148 (2015) 358-365.

[6] I. Jomaa, O. Noureddine, S. Gatfaoui, N. Issaoui, T. Roisnel, H. Marouani, Experimental, computational, and in silico analysis of $(C_8H_{14}N_2)_2[CdCl_6]$ compound, J. Mol. Struct. 1213 (2020) 128–186.

[7] S. Gatfaoui, N. Issaoui, S.A. Brandan, T. Roisnel, H. Marouani, Synthesis and characterization of p-xylylenediaminium bis(nitrate). Effects of the coordination modes of nitrate groups on their structural and vibrational properties, J. Mol. Struct. 1151 (2018) 152-168.

[8] H. Cheng, H. Li, (m-Phenylenedimethylene)diammonium dichloride, Acta Crystallogr. E64 (2008) o2060.

[9] A.Guesmi, T.Roisnel, H. Marouani, Featuring non-covalent interactions in m-xylylenediaminium bis(perchlorate) monohydrate: Synthesis, characterization and Hirshfeld surface analysis, J. Mol. Struct. 1194 (2019) 66–72.

[10] H. El Aribi, Y.J. Le Blanc, S. Antonsen, T. Sakuma, Analysis of perchlorate in foods and beverages by ion chromatography coupled with tandem mass spectrometry (IC- ESI-MS/MS), Anal. Chim. Acta 567 (1) (2006) 39-47.

[11] H.P. Wagner, B.V. Pepich, C. Pohl, D. Later, K. Srinivasan, R. Lin, B. Deborba, D.J. Munch, Selective method for the analysis of perchlorate in drinking water satnanograrn per liter levels, using two-dimensional ion chromatography with suppressed conductivity detection, J. Chromatogr. A 1155 (2007) 15-21.

[12] L. Chen, H. Chen, M. Shen, Z. Zhou, A. Ma, Analysis of perchlorate in milk powder and milk by hydrophilic interaction chromatography combined with tandem mass spectrometry, J. Agric. Food Chem. 58 (2010) 3736-3740.

[13] P. Winkler, M. Minteer, J. Willey, Analysis of perchlorate in water and soil by electrospray LC/MS/MS, Anal. Chem. 76 (2004) 469-473.

[14] L. Ye, H. You, J. Yao, X. Kang, L. Tang, Seasonal variation and factors influencing perchlorate in water, snow, soil and corns in Northeastern China, Chemosphere90 (2013) 2493-2498.

[15] R. Salmasi, A. Salimi, M. Gholizadeh, M. Rahmani, J.C. Garrison, Symmetric quaternary phosphonium cation and perchlorate/chlorate anions: crystal structure, Database study and Hirshfeld surface analysis, J. Mol. Struct. 1179 (2019) 549-557.

[16] C. Ben Mleh, T. Roisnel, H. Marouani, trans-2,5-Dimethylpiperazine-1,4-diium bis(perchlorate) dihydrate: crystal structure and Hirshfeld surface analysis, Acta Crystallogr. E72 (2015) 593-596.

[17] Bruker, APEX2, SAINT and SADABS, Bruker AXS Inc., Madison, Wisconsin, USA, 2006.

[18] G.M. Sheldrick, SHELXT–Integrated space-group and crystal-structure determination, Acta Crystallogr. A, 71 (2015) 3-8.

[19] G.M. Sheldrick, Crystal structure refinement with SHELXL, Acta Crystallogr., Sect. A: Found. Crystallogr. A, 64 (2008) 112-122.

[20] L.J. Farrugia, WinGX and ORTEP for windows: an update, J. Appl. Cryst. 45 (2012) 849-854.

[21] G. Bergerhoff, M. Berndt, K. Brandenburg, Evaluation of Crystallographic Data with the Program DIAMOND, J. Res. Natl. Inst. Stand. Technol., 101 (1996) 221–225.

[22] M.J. Frisch, G.W. Trucks, H.B. Schlegel, G.E. Scuseria, M.A. Robb, J.R. Cheese-man, G. Scalmani, V. Barone, B. Mennucci, G.A. Petersson, H. Nakatsuji, M. Car- icato, X. Li, H.P. Hratchian, A.F. Izmaylov, J. Bloino, G. Zheng, J.L. Sonnenberg, M. Hada, M. Ehara, K. Toyota, R. Fukuda, J. Hasegawa, M. Ishida, T. Nakajima, Y. Honda, O. Kitao, H. Nakai, T. Vreven, J.A. Montgomery Jr., J.E. Peralta, F. Ogliaro, M. Bearpark, J.J. Heyd, E. Brothers, K.N. Kudin, V.N. Staroverov, R. Kobayashi, J. Normand, K. Raghavachari, A. Rendell, J.C. Burant, S.S. Iyengar, J. Tomasi, M. Cossi, N. Rega, J.M. Millam, M. Klene, J.E. Knox, J.B. Cross, V. Bakken, C. Adamo, J. Jaramillo, R. Gomperts, R.E. Stratmann, O. Yazyev, A.J. Austin, R. Cammi, C. Pomelli, J.W. Ochterski, R.L. Martin, K. Morokuma, V.G. Zakrzewski, G.A. Voth, P. Salvador, J.J. Dannenberg, S. Dapprich, A.D. Daniels, O. Farkas, J.B. Foresman, J.V. Ortiz, J. Cioslowski, D.J. Fox, Gaussian, Inc., Wallingford CT, 2009.

[23] R. Dennington, T. Keith, J. Millam, GaussView, Version 5 (Semichem. Inc Shawnee Mission, KS, 2009)

[24] A.D. Becke, Becke's three parameter hybrid method using the LYP correlation functional, J. Chem. Phys. 98 (1993) 5648–5652.

[25] C. Lee, W. Yang, R.G. Parr, Development of the Colle-Salvetti correlation-energy formula into a functional of the electron density, Phys. Rev. (B37) (1988) 785–789.

[26] S.K. Wolff, D.J. Grimwood, J.J. McKinnon, D. Jayatilaka, M.A. Spackamn, Crystal-Explorer 3.1, University of Westren Australia, Perth, 2013 3.1.

[27] T. Lu, F. Chen, Multiwfn: a multifunctional wave function analyzer, J. Comput. Chem. 33 (2012) 580–592.

[28] W. Humphrey, A. Dalke, K. Schulten, VMD: visual molecular dynamics, J. Mol. Gr. 14 (1996) 33–38.

[29] M. Waqas Alam, M. Farhan, B. Souayeh, M. Aamir, M. Shuaib Khan, Synthesis, Crystal Structure, Density Functional Theory (DFT) Calculations and Molecular Orbital Calculations of 4-Bromoanilinium Perchlorate Single Crystal, Crystals 11 (2021) 1070.

[30] S. Hou, P. Ren, Y. Zeng, The crystal structure of 3-amino-5-carboxypyridin-1-ium perchlorate monohydrate, $C_6H_9ClN_2O_7$, Z. Kristallogr. NCS, 236 (2021) 727-728.

[31] J. Sanmartín, A.M. García-Deibe, M. Fondo, F. Novio, N. Ocampo, M.R. Bermejo, Syn–anti and anti–anti conformations of a diimine derived from p-xylylenediamine and its neutral CoII and ZnII dinuclear complexes, Inorg. Chim. Acta, 359 (2006) 3156-3166.

[32] A.H. Arkenbout, A. Meetsma, T.T.M. Palstra, (p-Phenylenedimethylene)diammonium dichloride, Acta Cryst. E 63 (2007) o869–o870.

[33] Y. Zhang, M. T. Han, p-Phenylenedimethanaminium dibromide. Acta Cryst. E, 66 (2010) o1865-o1865.

[34] J.H. Nelson, A.N. Sarjeant, A.J. Norquist, Poly[tris(p-xylylenediaminium) [tetradeca-l-oxo-hexadecanonamolybdate(VI)] dihydrate], Acta Cryst. E63 (2007) m1442-m1444.

[35] M. Tahenti, N. Issaoui, T. Roisnel, H. Marouani, Synthesis, characterization, and computational survey of a novel material template o-xylylenediamine, J. Iran. Chem. Soc. 1207 (2021) 1-16.

[36] I. Jomaa, N. Issaoui, T. Roisnel, H. Marouani, Insight into non-covalent interactions in a tetrachlorocadmate salt with promising NLO properties: Experimental and computational analysis, J. Mol. Struct. 1242 (2021) 130730.

[37] M. Tahenti, N. Issaoui, T. Roisnel, H. Marouani, O. Al-Dossary, Aleksandr S. Kazachenko, Self-assembly of a new cobalt complex, $(C_6H_{14}N_2)_3[CoCl_4]Cl$: Synthesis, empirical and DFT calculations, J. King Saud Univ. Sci. 34 (2022) 101807.

[38] D.S. Michael, M.K. Priya, J. Sidharthan, M. Kumar, R.V. Solomon, D.R. Jonathan, Synthesis, crystallography, DFT, MTT assay, and molecular docking studies of an exocyclic double-bonded crystalline chalcone, Chem. Data Collect. 36 (2021) 100773.

[39] I. Jomaa, N. Issaoui, T. Roisnel, H. Marouani, Assembly of two new hybrid chloride materials with potential NLO properties: Structure elucidation, empirical and computational studies, J. Iran. Chem. Soc. 1213 (2022) 1–16.

[40] R.P.Sukiasyan, K.Y.Suponitsky, A.K.Atanesyan, A.A.Danghyan, A.A.Hovhannisyan, A.M.Petrosyan, Crystal structures and vibrational spectra of L-argininium(2+) bis(tetrafluoroborate) and L-argininium(2+) bis(perchlorate), Spectrochim. Acta A Mol. Biomol. Spectrosc. 228 (2020) 117782.

[41] S.A. Brandán, Theoretical study of the structure and vibrational spectra of chromyl perchlorate, $CrO_2 (ClO_4)_2$, J. Mol. Struct.: THEOCHEM 908 (2009) 19–25.

[42] C. Daghar, N. Issaoui, T. Roisnel, V. Dorcet, H. Marouani, Empirical and computational studies on newly synthesis cyclohexylammonium perchlorate. J. Mol. Struct. 1230 (2021) 129820.

[43] C. Daghar, N. Issaoui, T. Roisnel, H. Marouani, O. Al-Dossary, Molecular structure, spectroscopy, quantum chemical and antibacterial activity investigations of 2-methylbenzylammonium perchlorate, J. Mol. Struct.1247 (2022) 131311.

[44] R. F. W. Bader , Atoms in Molecules, A Quantum Theory, Oxford University Press, Oxford, 1990 ISBN .

[45] T. Lu, F. Chen, Multiwfn: a multifunctional wavefunction analyzer, J. Comput. Chem. 33 (2012) 580–592 .

[46] I. Rozas, I. Alkorta, J. Elguero, Behavior of ylides containing N, O, and C atoms as hydrogen bond acceptors, J. Am. Chem. Soc. 122 (2000) 11154-11161.

[47] E.R. Johnson, S. Keinan, P. Mori-Sanchez, J. Contreras-García, A.J. Cohen, W. Yang, J. Am. Chem. Soc. 132 (2010) 6498-6506.

[48] J. Contreras-Garcia, W. Yang, E.R. Johnson, Analysis of hydrogen-bond interaction potentials from the electron density: integration of non covalent interaction regions, J. Phys. Chem. A 115 (2011) 12983-12990.

[49] N. Mohan, C.H. Suresh, A molecular electrostatic potential analysis of hydrogen, halogen and dihydrogen bonds, J. Phys. Chem. 118 (2014) 1697–1705.

[50] R.S. Mulliken, A new electroaffinity scale; together with data on valence states and on valence ionization potentials and electron affinities, J. Chem. Phys. 2 (1934) 782–794.

[51] R.G. Parr, L. von Szentpály, S. Liu, Electrophilicity index, J. Am. Chem. Soc. 121 (1999) 1922–1924.

Figure captions

Fig. 1. ORTEP representation of the asymmetric unit of $(C_8H_{14}N_2)(ClO_4)_2 \cdot H_2O$ with atom-labeling scheme. Displacement ellipsoids are drawn at the 50% probability level. Hydrogen bonds are denoted as dashed lines **(a)**. The optimized geometric model using the B3LYP/LanL2DZ method **(b)**.

Fig. 2. The packing of $(C_8H_{14}N_2)(ClO_4)_2 \bullet H_2O$ viewed down the a-axis, the inorganic part is given in space filling model **(a)**, and partial view of the crystal structure showing the anion and the bridging water molecules interacting through hydrogen bonds to produce a corrugated chain **(b)**.

Fig. 3. Projection of $(C_8H_{14}N_2)(ClO_4)_2 \cdot H_2O$ in the ab plane **(a)**, while **(b)** is the patterns of hydrogen bonding in the title compound. Carbon atoms were omitted for clarity of the projection along a perspective view, **(c)** represents a view highlighting intermolecular interactions between organic cations C–H…π stacking.

Fig. 4. 3D Hirshfeld surfaces mapped with d_{norm}**(a)**in the range [-0.409 - 1.182] (red dotted lines represent hydrogen bonds), view of the curvedness **(b)** and the shape index **(c)** plots of $(C_8H_{14}N_2)(ClO_4)_2 \cdot H_2O$.

Fig. 5. Experimental IR spectrum of $(C_8H_{14}N_2)(ClO_4)_2 \cdot H_2O$.

Fig. 6. Graphic representation of critical points within $(C_8H_{14}N_2)(ClO_4)_2 \cdot H_2O$ compound.

Fig. 7. Representation of different types of interactions **(a)** and graph of the reduced density gradient vs. sign $(\lambda_2)\rho$ of $(C_8H_{14}N_2)(ClO_4)_2 \cdot H_2O$ **(b)**.

Fig. 8. The 3-D electrostatic potential maps of $(C_8H_{14}N_2)(ClO_4)_2 \cdot H_2O$.

Fig. 9. Frontier molecular orbital plots of $(C_8H_{14}N_2)(ClO_4)_2 \cdot H_2O$.

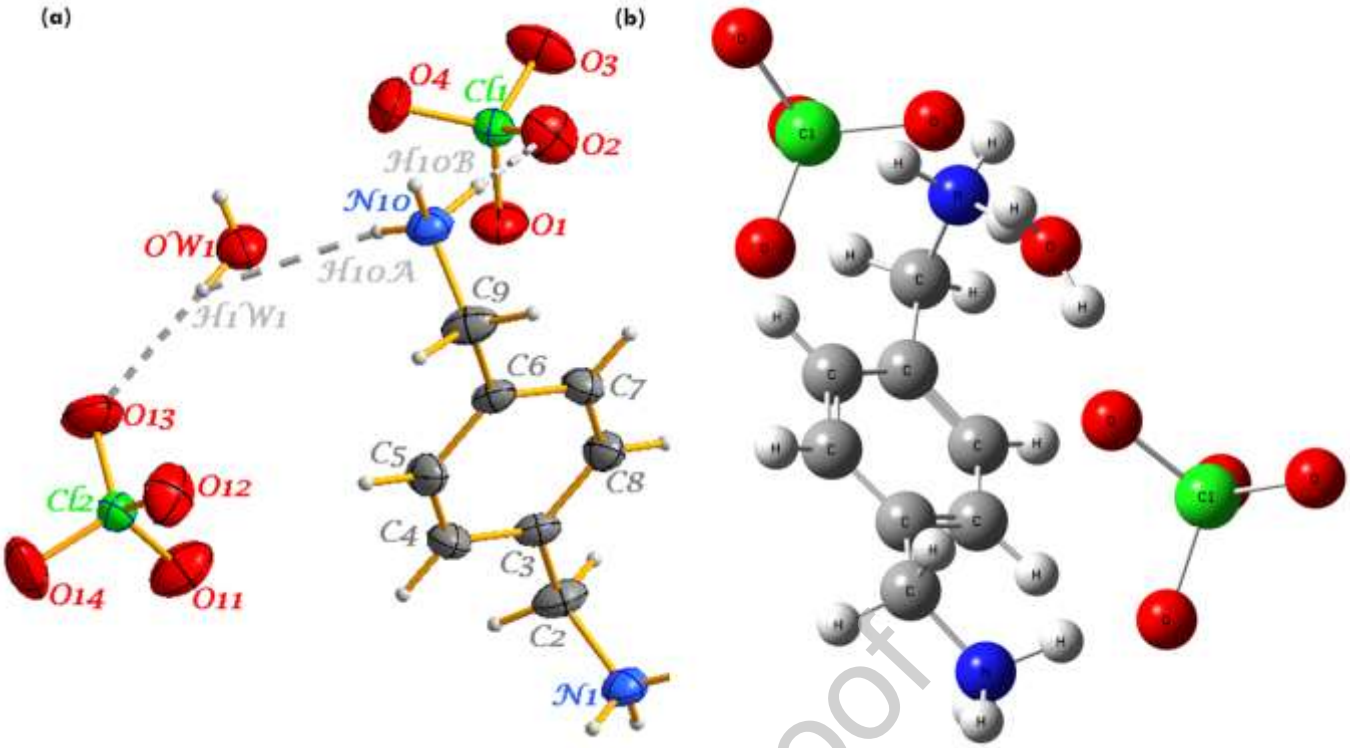

Fig. 1. ORTEP representation of the asymmetric unit of $(C_8H_{14}N_2)(ClO_4)_2 \cdot H_2O$ with atom-labeling scheme. Displacement ellipsoids are drawn at the 50% probability level. Hydrogen bonds are denoted as dashed lines **(a)**. The optimized geometric model using the B3LYP/LanL2DZ method **(b)**.

Table captions

Table 1. Crystal data and experimental parameters used for the intensity data collection strategy and final results of the structure determination.

Table 2. Principal intermolecular distances (Å) and bond angles (°) in $(C_8H_{14}N_2)(ClO_4)_2 \cdot H_2O$ by X-ray data (with estimated standard deviation in parentheses) and by theoretical calculations.

Table 3. Hydrogen-bonds details (Å, °).

Table 4. Topological parameters values of $(C_8H_{14}N_2)(ClO_4)_2 \cdot H_2O$.

Table 1. Crystal data and experimental parameters used for the intensity data collection strategy and final results of the structure determination.

N° CCDC	2150287
Chemical formula	$(C_8H_{14}N_2)(ClO_4)_2 \cdot H_2O$
Formula weight (g mol^{-1})	355.13
Crystal system, space group	Monoclinic, $P2_1/c$
Temperature (K)	150
a (Å)	5.1097 (7)
b (Å)	11.1037 (15)
c (Å)	25.380 (4)
β (°)	92.475 (5)
V ($Å^3$)	1438.6 (3)
Z	4
F(000)	736
μ (Mo *K*α)	0.50 mm^{-1}
Index ranges	$-6 \leq h \leq 6$, $-14 \leq k \leq 14$, $-33 \leq l \leq 26$
Reflections collected	8363
Independent reflections	3265
Reflections with $I > 2\sigma(I)$	2788
R_{int}	0.035
$(\sin \theta/\lambda)_{max}$ ($Å^{-1}$)	0.652
Absorption correction: multi-scan	T_{min}= 0.732, T_{max} = 0.887
Refined parameters	214
$R[F^2 > 2\sigma(F^2)]$	0.056
$wR(F^2)$	0.128
Goodness of fit	1.14
$\Delta\rho_{max}$, $\Delta\rho_{min}$ (e $Å^{-3}$)	0.36, −0.46

Table 2. Principal intermolecular distances (Å) and bond angles (°) in $(C_8H_{14}N_2)(ClO_4)_2 \cdot H_2O$ by X-ray data (with estimated standard deviation in parentheses) and by theoretical calculations.

Bond lengths (Å)			**Bond angles (°)**		
Calculated B3LYP/LanL2DZ		X-Ray	Calculated B3LYP/LanL2DZ		X-Ray
Inorganic atom position					
Cl1—O1	1.44	1.430 (2)	O1—Cl1—O2	107.2	109.16 (16)
Cl1—O2	1.49	1.440 (2)	O1—Cl1—O3	112.5	109.96 (17)
Cl1—O3	1.43	1.432 (3)	O4—Cl1—O1	110.3	108.93 (17)
Cl1—O4	1.47	1.419 (3)	O3—Cl1—O2	108.7	106.96 (16)
Cl2—O11	1.40	1.422 (3)	O4—Cl1—O2	108	110.23 (19)
Cl2—O12	1.44	1.441 (2)	O4—Cl1—O3	110	111.57 (19)
Cl2—O13	1.46	1.426 (2)	O11—Cl2—O12	107.7	108.80 (17)
Cl2—O14	1.42	1.424 (3)	O11—Cl2—O13	105	110.09 (18)
			O11—Cl2—O14	107.7	109.4 (2)
			O13—Cl2—O12	110.4	109.83 (17)
			O14—Cl2—O12	113.2	108.29 (19)
			O14—Cl2—O13	112.3	110.39 (18)
Organic atom position					
N1—C2	1.52	1.491 (4)	N1—C2—C3	112.6	112.8 (3)
N10—C9	1.53	1.487 (4)	N10—C9—C6	111	111.8 (2)
C2—C3	1.52	1.499 (4)	C4—C3—C8	119.2	118.9 (3)
C3—C8	1.40	1.391 (4)	C4—C3—C2	122.9	120.9 (3)
C4—C5	1.41	1.383 (4)	C8—C3—C2	117.6	120.1 (3)
C5—C6	1.41	1.392 (4)	C3—C4—C5	120.1	120.7 (3)
C6—C7	1.41	1.384 (4)	C4—C5—C6	120	120.5 (3)
C6—C9	1.52	1.502 (4)	C7—C6—C5	119.1	118.8 (3)
C7—C8	1.41	1.387 (4)	C7—C6—C9	120.6	120.7 (3)
			C5—C6—C9	120.4	120.5 (3)
			C6—C7—C8	120.2	120.7 (3)
			C7—C8—C3	120.5	120.4 (3)

Table 3. Hydrogen-bonds details (Å, °).

D—H···*A*	*D*—H(Å)	H···*A*(Å)	*D*···*A*(Å)	*D*—H···*A*(Å)
N1—H1*A*···O3^{i}	0.87 (4)	2.38 (4)	3.088 (4)	139 (3)
N1—H1*A*···O4^{ii}	0.87 (4)	2.42 (4)	2.856 (4)	112 (3)
N1—H1*A*···O14^{iii}	0.87 (4)	2.47 (4)	2.921 (4)	113 (3)
N1—H1*B*···O12^{iv}	0.91 (4)	2.26 (4)	3.159 (4)	172 (3)
N1—H1*C*···O2^{v}	0.83 (4)	2.56 (4)	3.123 (4)	127 (3)
N1—H1*C*···O3^{v}	0.83 (4)	2.31 (4)	3.133 (4)	177 (4)
N10—H10*A*···O*W*1	0.84 (4)	2.09 (4)	2.926 (4)	175 (4)
N10—H10*B*···O2	0.98 (4)	2.08 (4)	3.008 (4)	157 (3)
N10—H10*C*···O*W*1^{vi}	0.92 (4)	2.29 (4)	3.044 (4)	139 (3)
O*W*1—H1*W*1···O13	0.83 (5)	2.25 (5)	2.969 (4)	145 (4)
O*W*1—H2*W*1···O12^{vii}	0.72 (5)	2.33 (5)	3.040 (4)	167 (5)
C2—H2B···O1^{i}	0.99	2.54	3.482 (5)	159
C2–H2A…Cg^{viii}	0.99	3.12	3.812	128
C9–H9B…Cg^{vi}	0.98	3.00	3.849	143

Symmetry codes: (i) −x, −y+1, −z+1; (ii) x, y−1, z; (iii) −x, y−1/2, −z+3/2; (iv) −x+1, y−1/2, −z+3/2; (v) −x+1, −y+1, −z+1; (vi) x+1, y, z; (vii) −x+1, y+1/2, −z+3/2; (viii) x-1, y,z.

Cg: the centroid of the benzene ring

Table 4. Topological parameters values of $(C_8H_{14}N_2)(ClO_4)_2 \cdot H_2O$.

Interaction	$\nabla^2\rho(r)$ (u. a)	$\rho(r)$ (u. a)	G(r) (u. a)	V(r) (u. a)	H(r) (u. a)	ε	$E_{interaction}$ (kJ.mol^{-1})
RCP	0.0226	0.1665	0.0340	-0.0264	0.0076	-1.2075	-
NRCP1	0.0031	0.0139	0.0026	-0.0018	0.0009	-2.0792	-
NRCP2	0.0009	0.0040	0.0007	-0.0004	0.0003	-1.2870	-
NRCP3	0.0023	0.0107	0.0020	-0.0014	0.0007	-1.7875	-
NRCP4	0.0034	0.0017	0.0027	-0.0019	0.0008	-1.4041	-
C_{14}-H_{15}...O_{27}	0.0043	0.0160	0.0032	-0.0023	0.0008	0.4591	-3.02
C_{11}-H_{12}...O_{32}	0.0061	0.0194	0.0041	-0.0033	0.0008	0.0345	-4.33
C_9-H_{10}...O_{31}	0.0037	0.0145	0.0029	-0.0021	0.0008	0.3742	-2.76
N_{21}-H_{22}...O_{35}	0.0193	0.0722	0.0154	-0.0128	0.0026	0.0646	-16.80
O_{35}-H_{36}...O_{33}	0.0126	0.0488	0.0104	-0.0086	0.0018	0.1091	-11.30
N_{21}-H_{23}...O_{27}	0.0196	0.0638	0.0143	-0.01254	0.0017	0.0634	-16.46

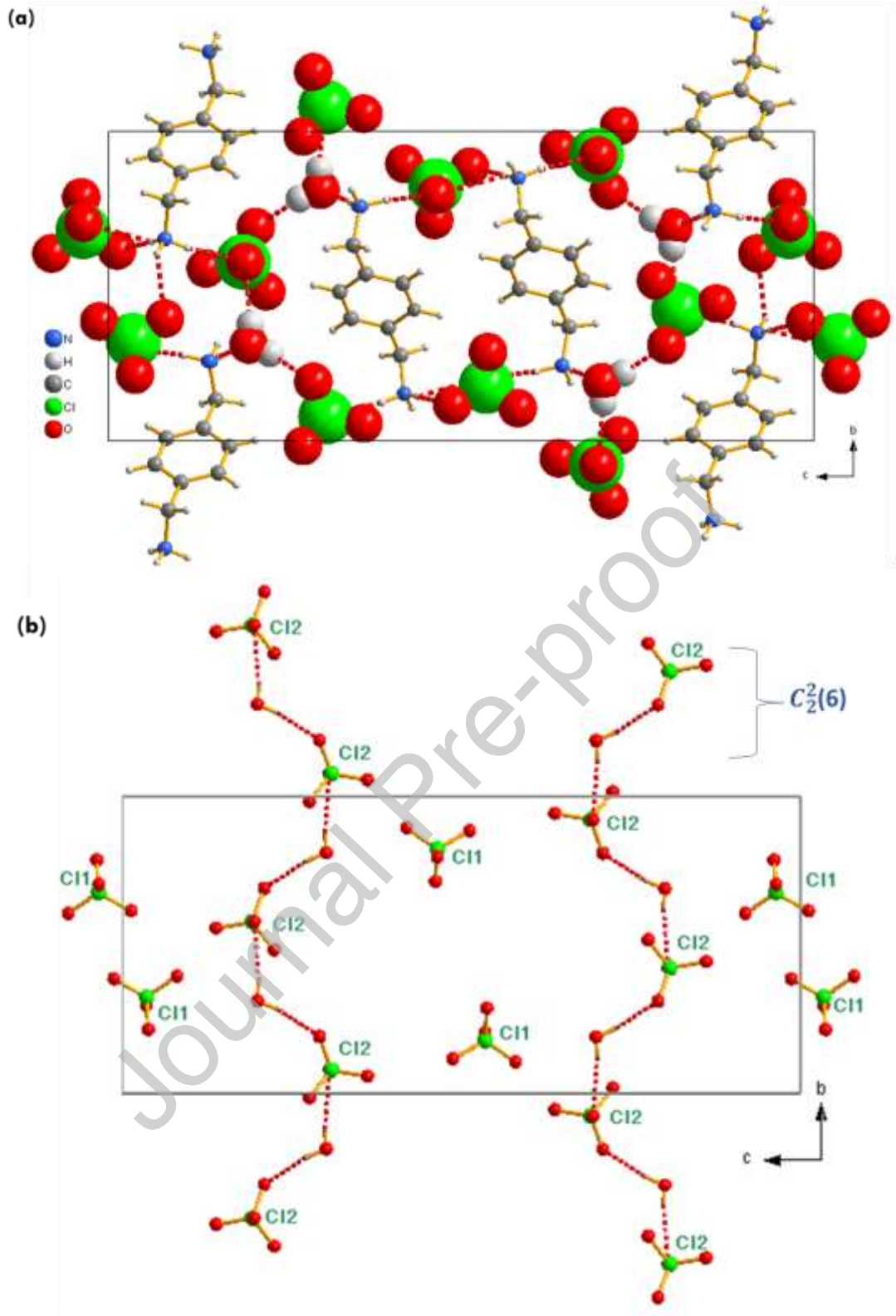

Fig. 2. The packing of $(C_8H_{14}N_2)(ClO_4)_2 \cdot H_2O$ viewed down the a-axis, the inorganic part is given in space filling model **(a)**, and partial view of the crystal structure showing the anion and the bridging water molecules interacting through hydrogen bonds to produce a corrugated chain **(b)**.

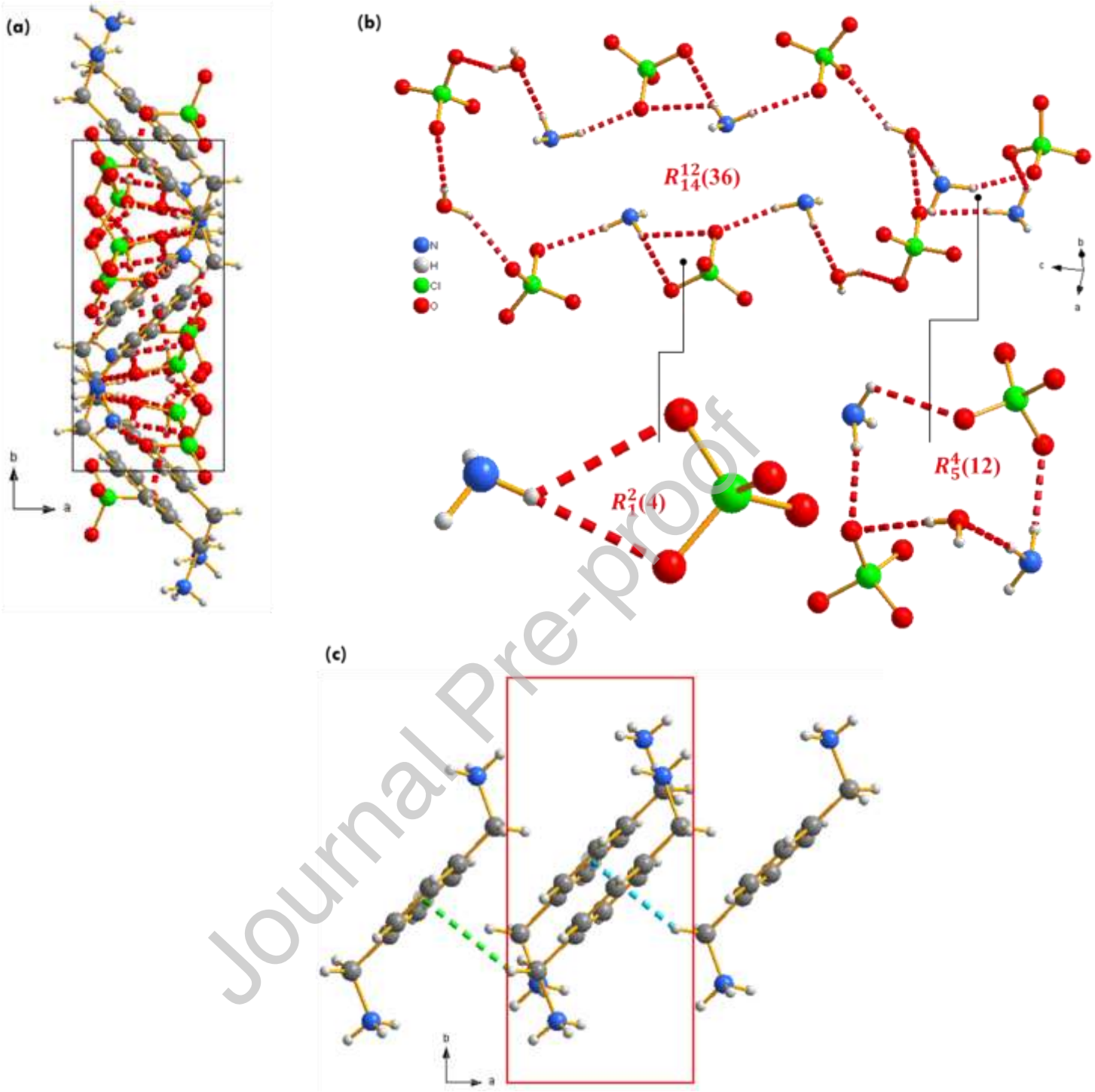

Fig. 3. Projection of $(C_8H_{14}N_2)(ClO_4)_2{\cdot}H_2O$ in the ab plane **(a)**, while **(b)** is the patterns of hydrogen bonding in the title compound. Carbon atoms were omitted for clarity of the projection along a perspective view, **(c)** represents a view highlighting intermolecular interactions between organic cations C–H…π stacking.

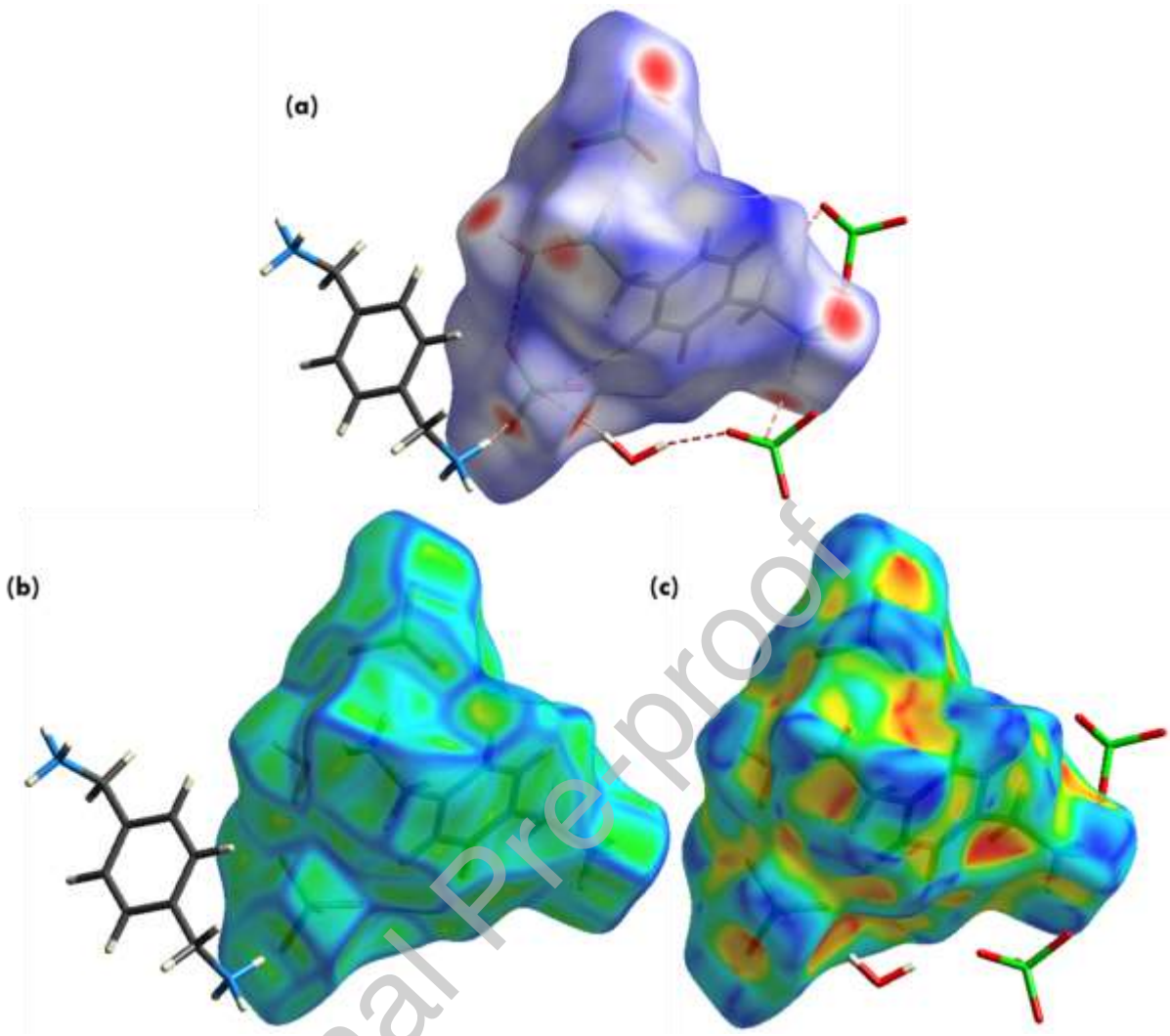

Fig. 4. 3D Hirshfeld surfaces mapped with d_{norm}**(a)**in the range [-0.409 - 1.182] (red dotted lines represent hydrogen bonds), view of the curvedness **(b)** and the shape index **(c)** plotsof $(C_8H_{14}N_2)(ClO_4)_2{\cdot}H_2O$.

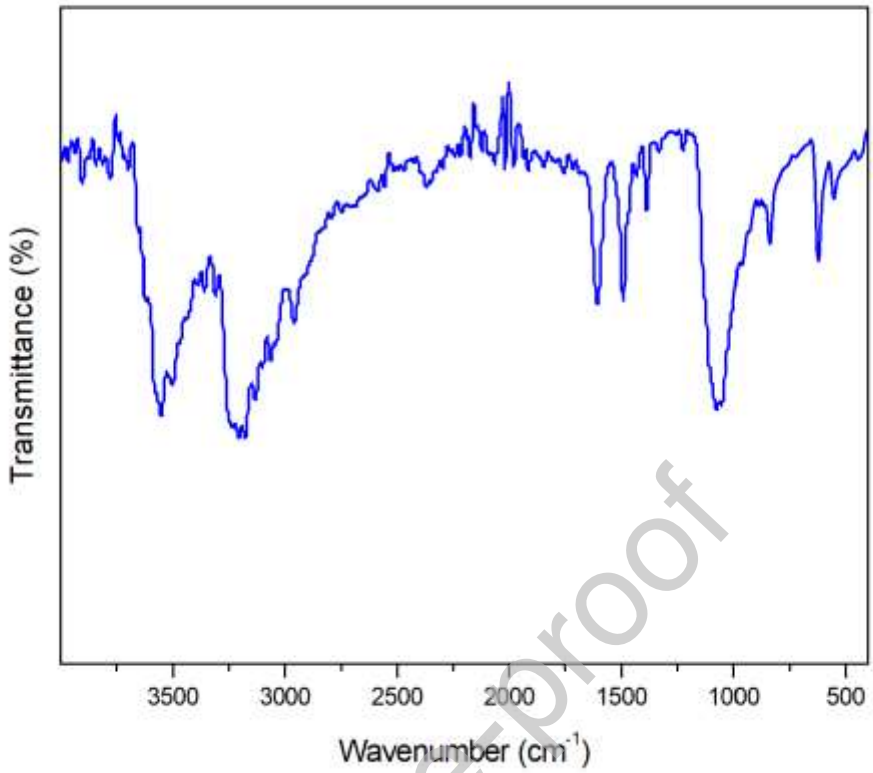

Fig. 5. Experimental IR spectrum of $(C_8H_{14}N_2)(ClO_4)_2 \cdot H_2O$.

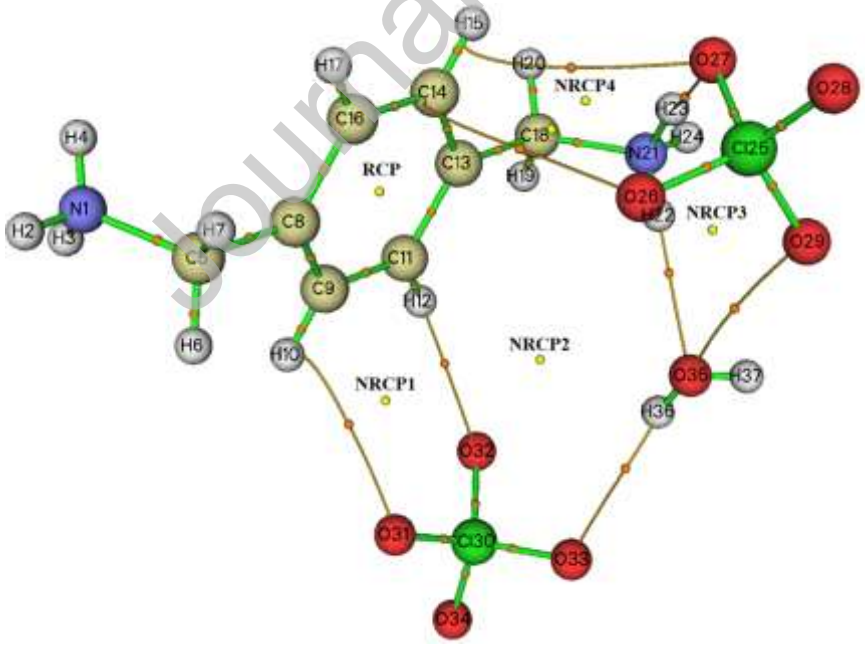

Fig. 6. Graphic representation of critical points within $(C_8H_{14}N_2)(ClO_4)_2 \cdot H_2O$ compound.

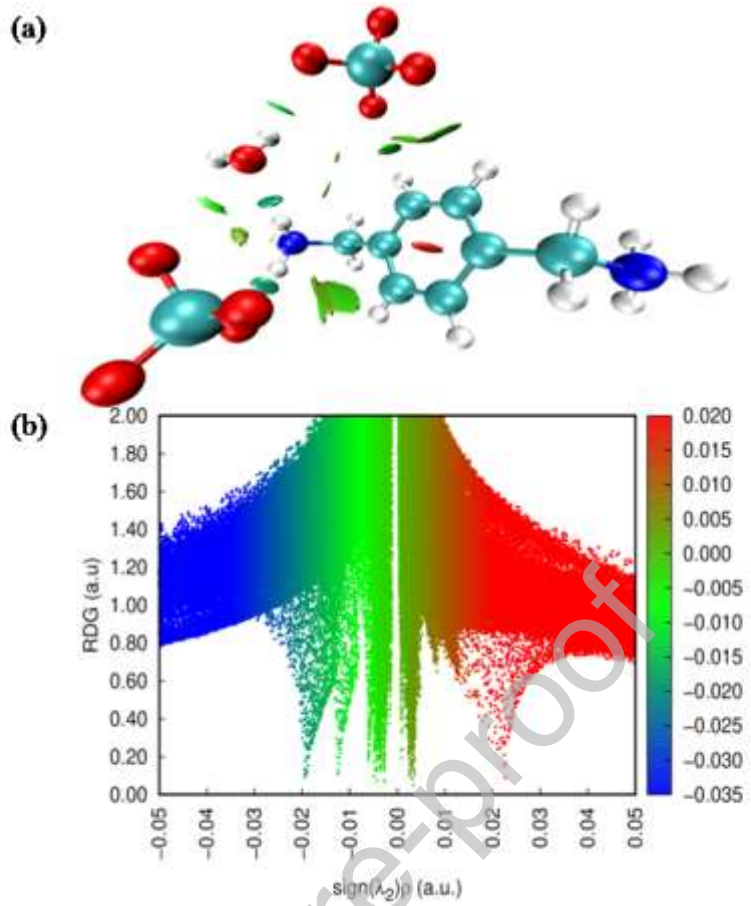

Fig. 7. Representation of different types of interactions **(a)** and graph of the reduced density gradient vs. sign $(\lambda_2)\rho$ of $(C_8H_{14}N_2)(ClO_4)_2 \cdot H_2O$ **(b)**.

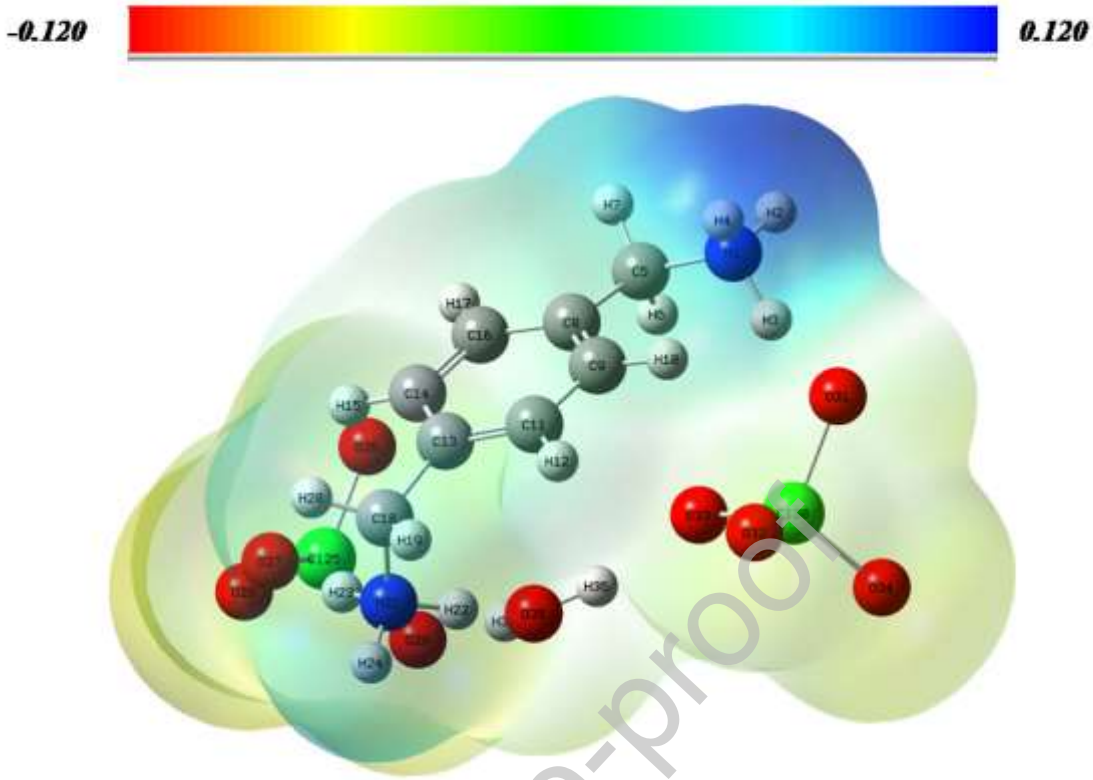

Fig. 8. The 3-D electrostatic potential maps of $(C_8H_{14}N_2)(ClO_4)_2 \cdot H_2O$.

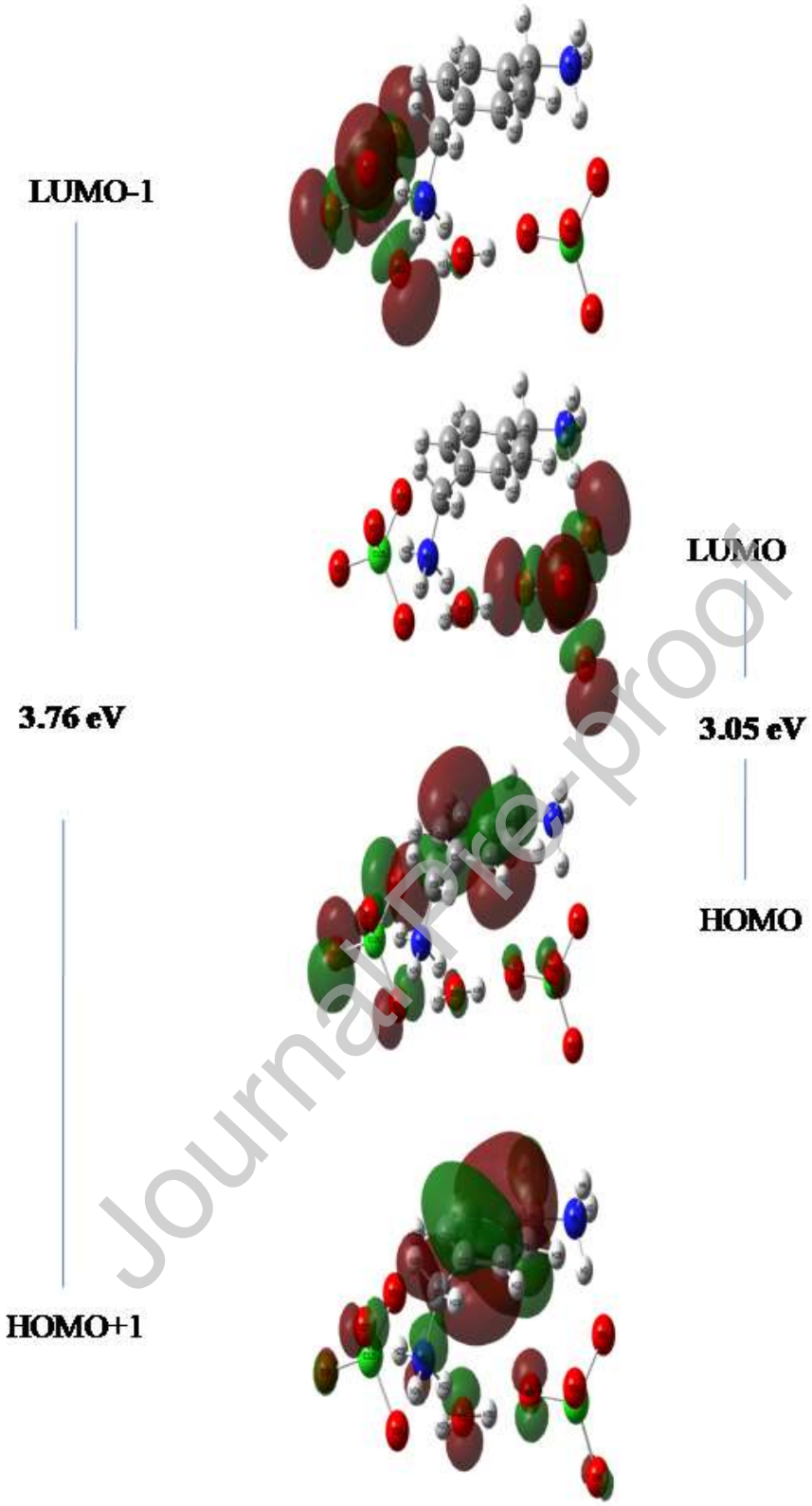

Fig. 9. Frontier molecular orbital plots of $(C_8H_{14}N_2)(ClO_4)_2 \cdot H_2O$.